JAERI-M
87-127

ICRF-ENHANCEMENT OF BEAM-INDUCED TAIL TEMPERATURE

August 1987

Mitsuru YAMAGIWA, Tomonori TAKIZUKA,
Haruyuki KIMURA and Masafumi AZUMI

日本原子力研究所
Japan Atomic Energy Research Institute

JAERI-Mレポートは，日本原子力研究所が不定期に公刊している研究報告書です。
入手の問合わせは，日本原子力研究所技術情報部情報資料課（〒319-11茨城県那珂郡東海村）あて，お申しこしください。なお，このほかに財団法人原子力弘済会資料センター（〒319-11 茨城県那珂郡東海村日本原子力研究所内）で複写による実費頒布をおこなっております。

JAERI-M reports are issued irregularly.
Inquiries about availability of the reports should be addressed to Information Division Department of Technical Information, Japan Atomic Energy Research Institute, Tokai-mura, Naka-gun, Ibaraki-ken 319-11, Japan.

編集兼発行　日本原子力研究所
印　　刷　㈱高野高速印刷

ICRF-ENHANCEMENT OF BEAM-INDUCED TAIL TEMPERATURE

Mitsuru YAMAGIWA, Tomonori TAKIZUKA, Haruyuki KIMURA+
and Masafumi AZUMI+

Department of Thermonuclear Fusion Research
Naka Fusion Research Establishment
Japan Atomic Energy Research Institute
Naka-machi, Naka-gun, Ibaraki-ken

(Received July 28, 1987)

Enhancement of temperature of the beam-induced ion tail due to second harmonic ICRF (ion cyclotron range of frequency) waves is investigated. The ion distribution function is calculated analytically by use of a Fokker-Planck equation combined with the beam source and quasi-linear RF (radio-frequency) diffusion terms. A simple scaling of the "extended-tail temperature" with respect to the deposited RF power density is presented. Comparison is made with numerical results by using a two-dimensional Fokker-Planck code. It is found that the numerical results for beam injection nearly-perpendicular to the magnetic field are in good agreement with the analytical ones. Also discussed is comparison with the experimental data.

Keywords; Extended-Tail Temperature, Ion Tail Formation, Second Harmonic Ion Cyclotron Range of Frequency Wave, ICRF Heating, Neutral-Beam Injection, Beam-Induced Tail, Fokker-Planck Equation, Quasi-Linear RF Diffusion, Magnetically Confined Plasma

---

+ Department of Large Tokamak Research

イオンサイクロトロン波によるビーム誘起テイル温度の向上

日本原子力研究所那珂研究所核融合研究部
山極　満・滝塚　知典・木村　晴行[+]・安積　正史[+]

（１９８７年７月２８日受理）

イオンサイクロトロン第２高調波によるビーム誘起イオンテイル温度の向上について研究する。ビーム源および準線型高周波拡散項を含むフォッカープランク方程式を用いてイオン分布関数を解析的に計算する。高周波吸収パワー密度に関する〝拡張テイル温度〟の簡単な比例則が呈示される。２次元フォッカープランクコードを用いた数値計算結果との比較がなされる。ビームが磁場に対して直角近くに入射される場合，数値計算結果と解析結果との間に良い一致が見られる。実験データとの比較検討もなされる。

那珂研究所：　３１１−０２　茨城県那珂郡那珂町大字向山８０１−１
＋　臨界プラズマ研究部

CONTENTS

目　　次

1. INTRODUCTION

The most successful heating methods in magnetically confined plasmas are neutral-beam injection (NBI) and ion cyclotron range of frequency (ICRF) heating. During the combination of NBI and ICRF heating, high energy ions induced by NBI are accelerated by ICRF waves. The tail is extended to the energy region above the injection energy by radio-frequency(RF)-induced diffusion. This acceleration by the ICRF waves was studied in terms of the ICRF-enhancement of the beam-driven current [1,2] and of the fusion reactivity [3-5].

Efficient ion heating was observed in the NBI plus ICRF heating experiments on PLT [6]. Recent experiments on combined NBI and ICRF heating in JET [7] and JT-60 [8,9] indicated significant beam acceleration by ICRF: The increase of the "extended-tail temperature" was demonstrated.

It is useful to describe this increase of the "extended-tail temperature" as a function of the RF power density for the experimental data analyses and the control of the ion distribution function. In this paper we analytically and numerically study effects of the ICRF waves on the ion distribution function with the beam-induced tail, and obtain a scaling of the "extended-tail temperature" with respect to the deposited RF power density. The analyses are based on a local Fokker-Planck equation.

In Section 2 the angle-averaged distribution function of ions with the tail for combined NBI and second harmonic ICRF heating is derived analytically. A scaling of the "extended-tail temperature" with respect to the deposited RF power density is presented in Section 3. In Section 4 numerical analyses are performed by using a two-dimensional Fokker-Planck code, and analytical and numerical results are compared. In Section 5 comparison with the data of the combined heating experiments in JT-60 is discussed. Section 6 contains the conclusion.

2. ANGLE-AVERAGED DISTRIBUTION

In this section, we analytically study the ion tail formation during combined NBI and second harmonic ICRF heating. We use a local Fokker-Planck equation with the beam source and quasi-linear RF diffusion terms. A linearized Fokker-Planck collision operator is adopted, since emphasis is placed on RF effects on the high energy tail. Trapped particle effects on the tail formation are not taken into account in the present calculation. The time evolution of the ion distribution function, f, during

1. INTRODUCTION

The most successful heating methods in magnetically confined plasmas are neutral-beam injection (NBI) and ion cyclotron range of frequency (ICRF) heating. During the combination of NBI and ICRF heating, high energy ions induced by NBI are accelerated by ICRF waves. The tail is extended to the energy region above the injection energy by radio-frequency(RF)-induced diffusion. This acceleration by the ICRF waves was studied in terms of the ICRF-enhancement of the beam-driven current [1,2] and of the fusion reactivity [3-5].

Efficient ion heating was observed in the NBI plus ICRF heating experiments on PLT [6]. Recent experiments on combined NBI and ICRF heating in JET [7] and JT-60 [8,9] indicated significant beam acceleration by ICRF: The increase of the "extended-tail temperature" was demonstrated.

It is useful to describe this increase of the "extended-tail temperature" as a function of the RF power density for the experimental data analyses and the control of the ion distribution function. In this paper we analytically and numerically study effects of the ICRF waves on the ion distribution function with the beam-induced tail, and obtain a scaling of the "extended-tail temperature" with respect to the deposited RF power density. The analyses are based on a local Fokker-Planck equation.

In Section 2 the angle-averaged distribution function of ions with the tail for combined NBI and second harmonic ICRF heating is derived analytically. A scaling of the "extended-tail temperature" with respect to the deposited RF power density is presented in Section 3. In Section 4 numerical analyses are performed by using a two-dimensional Fokker-Planck code, and analytical and numerical results are compared. In Section 5 comparison with the data of the combined heating experiments in JT-60 is discussed. Section 6 contains the conclusion.

2. ANGLE-AVERAGED DISTRIBUTION

In this section, we analytically study the ion tail formation during combined NBI and second harmonic ICRF heating. We use a local Fokker-Planck equation with the beam source and quasi-linear RF diffusion terms. A linearized Fokker-Planck collision operator is adopted, since emphasis is placed on RF effects on the high energy tail. Trapped particle effects on the tail formation are not taken into account in the present calculation. The time evolution of the ion distribution function, f, during

NBI and second harmonic ICRF heating under the influence of Coulomb collisions is given by

$$\frac{\partial f}{\partial t} = \left(\frac{\partial f}{\partial t}\right)_{FP} + \left(\frac{\partial f}{\partial t}\right)_{QL} + S \ . \tag{1}$$

The first term on the right hand side of Eq.(1) is the linearized Fokker-Planck term,

$$\left(\frac{\partial f}{\partial t}\right)_{FP} = \frac{1}{v^2}\frac{\partial}{\partial v}\left\{ \alpha(v) f(v,\xi) + \beta(v)\frac{\partial}{\partial v} f(v,\xi) \right\}$$

$$+ \frac{1}{v^2}\frac{\partial}{\partial \xi}\left\{ \gamma(v,\xi)\sqrt{1-\xi^2}\frac{\partial}{\partial \xi} f(v,\xi) \right\} , \tag{2}$$

where v and ξ are the particle speed and cosine of the pitch-angle in spherical polar coordinates, respectively, and $\alpha(v)$, $\beta(v)$, and $\gamma(v,\xi)$ are the usual linearized Fokker-Planck coefficients [5,10]. The second term is the quasi-linear diffusion term due to ICRF waves,

$$\left(\frac{\partial f}{\partial t}\right)_{QL} = \frac{1}{v_\perp}\frac{\partial}{\partial v_\perp}\left(v_\perp D_\perp \frac{\partial}{\partial v_\perp} f(v,\xi) \right) , \tag{3}$$

where $v_\perp$ is the velocity component perpendicular to the magnetic field. The perpendicular diffusion coefficient due to the second harmonic ICRF waves, $D_\perp$, is given by

$$D_\perp = \frac{\omega_{ci}^2}{k_\perp^2 \tau_s}\hat{K}_2 \ J_1^2\left(\frac{k_\perp v_\perp}{\omega_{ci}}\right) , \tag{4}$$

where ω_{ci} is the ion cyclotron frequency and J_1 the Bessel function of the first kind of order one. The slowing-down time of an ion for collisions with electrons is represented as

$$\tau_s = 2.0\times10^{13}\ \frac{T_e^{3/2}}{n_e \ln\Lambda}\ \times\frac{A_i}{Z_i^2} , \tag{5}$$

where τ_s is in unit of sec, the electron temperature, T_e, is in keV, the electron density, n_e, is in cm^{-3}, $\ln\Lambda$ denotes the Coulomb logalithm, A_i the mass number, and Z_i the charge number of an ion. The normalized coefficient, $\hat{K}_2$, is proportional to the square of wave amplitude. In the

present calculation, however, $\hat{K}_2$ is given as an external parameter. The perpendicular wave number of the ICRF wave, $k_\perp$, is determined from the cold plasma dispersion relation [11],

$$\frac{c^2 k_\perp^2}{\omega^2} = K_\perp - \frac{K_\times^2}{K_\perp} \quad , \tag{6}$$

where c is the speed of light, $\omega = 2\omega_{ci}$ is the frequency of the RF wave, and $K_\perp$ and $K_\times$ are the well-known components of the cold plasma dielectric tensor [12].

The source term, S, originates from NBI;

$$S = \frac{P_{\mathrm{NBI}}}{2\pi E_0 v^2} \delta(v - v_0)\ p(\xi) \quad . \tag{7}$$

where P_{NBI} is the deposited beam power density, the monochromatic injection energy of $E_0 = m_i v_0^2/2$ is assumed, and $p(\xi)$ denotes the distribution function with respect to the injection angle ($\int p(\xi)\mathrm{d}\xi = 1$). The particle loss is assumed to occur in the very low energy region.

By averaging Eq.(1) in the steady state over ξ and truncating the Legendre expansion of f at zero order, we obtain the following normalized equation [4,5],

$$\frac{\mathrm{d}}{\mathrm{dv}} F_0(\mathrm{v}) + A(\mathrm{v}) F_0(\mathrm{v}) = B(\mathrm{v}) U(\mathrm{v}_0 - \mathrm{v}) \quad , \tag{8}$$

where

$$F_0(\mathrm{v}) = \frac{1}{2} \int_{-1}^{1} \mathrm{d}\xi\ f(v, \xi) \times \frac{v_i^3}{n_i} \quad , \tag{9}$$

$$A(\mathrm{v}) = \frac{\alpha(v)\tau_s / v_i^3}{\beta(v)\tau_s / v_i^4 + \hat{K}_2 \mathrm{v}^2 C(\mathrm{v}) / k_\perp^2 \rho_i^2} \quad , \tag{10}$$

$$B(\mathrm{v}) = \frac{P_{\mathrm{NBI}} \tau_s}{4\pi n_i E_0} \frac{1}{\beta(v)\tau_s / v_i^4 + \hat{K}_2 \mathrm{v}^2 C(\mathrm{v}) / k_\perp^2 \rho_i^2} \quad , \tag{11}$$

$$C(\mathrm{v}) = \int_0^1 \mathrm{d}\xi\ (1-\xi^2)\ J_1^2\left(k_\perp \rho_i \mathrm{v} \sqrt{1-\xi^2}\right) \quad , \tag{12}$$

and $U(\mathrm{v}_0 - \mathrm{v})$ is the step function. In the above equations, $v_i = \sqrt{T_i/m_i}$ is the ion thermal speed (T_i is the bulk ion temperature and m_i the ion mass), $\mathrm{v} = v/v_i$ is the normalized speed, n_i is the ion density, and

$\rho_i = v_i/\omega_{ci}$ is the Larmor radius of the thermal ion. The solution to Eq.(8) is expressed as

$$F_0(v \leqq v_0) = \exp\left(-\int_0^v dv'\ A(v')\right) \times \left\{ F_0(0) + \int_0^v dv'\ B(v')\ \exp\left(\int_0^{v'} dv''\ A(v'')\right) \right\}, \qquad (13a)$$

$$F_0(v \geqq v_0) = \exp\left(-\int_0^v dv'\ A(v')\right) \times \left\{ F_0(0) + \int_0^{v_0} dv'\ B(v')\ \exp\left(\int_0^{v'} dv''\ A(v'')\right) \right\}, \qquad (13b)$$

where the value of $F_0(0)$ is determined from the constraint of particle conservation.

The deposited power density, P, is normalized by n_iT_i/τ_s and is expressed as

$$\hat{P} = \frac{\tau_s}{n_iT_i}P = \frac{1.25\times10^3\ A_i\sqrt{T_e}}{10^{-26}n_e^2\ Z_i^2 \ln\Lambda}\ \frac{n_eT_e}{n_iT_i}\ P\ , \qquad (14)$$

where T is in keV, n is in cm^{-3}, and P is in W/cm^3. The normalized RF power density is given by

$$\hat{P}_{RF} = -\frac{4\pi\hat{K}_2}{k_\perp^2\rho_i^2}\int_0^\infty dv\ v^3\ C(v)\ \frac{dF_0(v)}{dv}\ . \qquad (15)$$

Figure 1 shows the angle-averaged energy distribution function of ions, $F_0(v^2/2)$, for combined NBI and second harmonic ICRF heating. The ratio of the electron temperature to the ion temperature is chosen as $T_e/T_i = 1.1$. The NBI parameters are $E_0/T_i = 20$ and $\hat{P}_{NBI} = 4$. The RF parameter, $\hat{K}_2$, is varied as (a) 0, (b) 0.5, (c) 1.0, and (d) 1.5, and the wave number is set $k_\perp\rho_i = 0.064 \ll 1$. The figure shows the beam-induced tail in the region, $8 < v^2/2 < 20$, and the extension of this tail to the high energy region, $v^2/2 > 20$, by the ICRF wave. The ordinate is the natural logarithm of F_0. The extension of the beam-induced tail is measured by the "extended-tail temperature", $T_{1/e}$, which is defined as the e-folding energy from the injection energy;

$$F_0\left(\frac{v_0^2}{2}+\hat{T}_{1/e}\right) = \frac{1}{e}\ F_0\left(\frac{v_0^2}{2}\right)\ , \qquad (16)$$

where $T_{1/e}$ is normalized by T_i as $\hat{T}_{1/e} = T_{1/e}/T_i$. When the ICRF wave is absent, the beam-induced tail is spread beyond the injection energy by Coulomb collisions. We represent the e-folding energy from E_0 for this case as $T_{1/e}^{beam}$. We also introduce the increment of the "extended-tail temperature", $\Delta T_{1/e}$, defined as

$$\Delta T_{1/e} = T_{1/e} - T_{1/e}^{beam} , \tag{17}$$

which characterizes the effect of RF-induced diffusion on the beam-induced tail. From the figure, we get the following results; (a) $\hat{T}_{1/e}^{beam} = 1.08$, (b) $\Delta\hat{T}_{1/e} = 1.62$, (c) $\Delta\hat{T}_{1/e} = 3.44$, and (d) $\Delta\hat{T}_{1/e} = 5.50$. The deposited RF power density, $\hat{P}_{RF}$, is (b) 1.55, (c) 3.61, and (d) 7.28.

Figure 2 shows the dependence of $\hat{P}_{RF}$ on $\hat{K}_2$. Parameters are the same as those for Fig.1 except values of $\hat{K}_2$. The line (a) denotes $\langle\hat{P}_{RF}\rangle_M$ (= 2 $\hat{K}_2$) for the fixed Maxwellian distribution, the line (b) denotes $\langle\hat{P}_{RF}\rangle_B$ for the fixed distribution with only beam-induced tail (Fig.1(a)), and the line (c) is $\hat{P}_{RF}$ for the exact distribution given by Eq.(13). Deviation of $\hat{P}_{RF}$ from $\langle\hat{P}_{RF}\rangle_B$ becomes appreciable with the increase of $\hat{K}_2$.

3. SCALING OF EXTENDED-TAIL TEMPERATURE

In this section we derive a scaling of $\Delta T_{1/e}$ with respect to P_{RF}. At first, the relation between $\hat{K}_2$ and $\Delta\hat{T}_{1/e}$ is derived. The angle-averaged distribution function, $F_0(v)$, for $v \geqq v_0$, given by Eq.(13b) is rewritten as

$$F_0(v) = F_0(v_0) \exp\left(- \int_{v_0}^{v} dv' \, A(v') \right) . \tag{18}$$

Under the approximation, $\sqrt{T_i/m_i} \ll v \ll \sqrt{T_e/m_e}$ and $J_1^2(k_\perp v_\perp/\omega_{ci}) \simeq (k_\perp v_\perp/2\omega_{ci})^2$, the functions $A(v)$ and $C(v)$ can be reduced to

$$A(v) \simeq \frac{v\,(\,v^3 + v_c^3\,)}{\frac{T_e}{T_i}v^3 + v_c^3 + \frac{2}{15}\hat{K}_2 v^5} \equiv v\,G(\varepsilon) , \tag{19}$$

$$C(v) \simeq \frac{2}{15} k_\perp^2 \rho_i^2 v^2 , \tag{20}$$

where $\varepsilon = v^2/2$ is the normalized energy, and a function, $G(\varepsilon)$, is introduced for simplicity. The critical energy of an ion, $E_c = m_i v_c^2/2 = v_c^2 T_i/2$, below

where $T_{1/e}$ is normalized by T_i as $\hat{T}_{1/e} = T_{1/e}/T_i$. When the ICRF wave is absent, the beam-induced tail is spread beyond the injection energy by Coulomb collisions. We represent the e-folding energy from E_0 for this case as $T_{1/e}^{beam}$. We also introduce the increment of the "extended-tail temperature", $\Delta T_{1/e}$, defined as

$$\Delta T_{1/e} = T_{1/e} - T_{1/e}^{beam} , \tag{17}$$

which characterizes the effect of RF-induced diffusion on the beam-induced tail. From the figure, we get the following results; (a) $\hat{T}_{1/e}^{beam} = 1.08$, (b) $\Delta\hat{T}_{1/e} = 1.62$, (c) $\Delta\hat{T}_{1/e} = 3.44$, and (d) $\Delta\hat{T}_{1/e} = 5.50$. The deposited RF power density, $\hat{P}_{RF}$, is (b) 1.55, (c) 3.61, and (d) 7.28.

Figure 2 shows the dependence of $\hat{P}_{RF}$ on $\hat{K}_2$. Parameters are the same as those for Fig.1 except values of $\hat{K}_2$. The line (a) denotes $\langle\hat{P}_{RF}\rangle_M$ (= 2 $\hat{K}_2$) for the fixed Maxwellian distribution, the line (b) denotes $\langle\hat{P}_{RF}\rangle_B$ for the fixed distribution with only beam-induced tail (Fig.1(a)), and the line (c) is $\hat{P}_{RF}$ for the exact distribution given by Eq.(13). Deviation of $\hat{P}_{RF}$ from $\langle\hat{P}_{RF}\rangle_B$ becomes appreciable with the increase of $\hat{K}_2$.

3. SCALING OF EXTENDED-TAIL TEMPERATURE

In this section we derive a scaling of $\Delta T_{1/e}$ with respect to P_{RF}. At first, the relation between $\hat{K}_2$ and $\Delta\hat{T}_{1/e}$ is derived. The angle-averaged distribution function, $F_0(v)$, for $v \geqq v_0$, given by Eq.(13b) is rewritten as

$$F_0(v) = F_0(v_0) \exp\left(- \int_{v_0}^{v} dv' \, A(v') \right) . \tag{18}$$

Under the approximation, $\sqrt{T_i/m_i} \ll v \ll \sqrt{T_e/m_e}$ and $J_1^2(k_\perp v_\perp/\omega_{ci}) \simeq (k_\perp v_\perp/2\omega_{ci})^2$, the functions $A(v)$ and $C(v)$ can be reduced to

$$A(v) \simeq \frac{v\,(v^3 + v_c^3)}{\frac{T_e}{T_i} v^3 + v_c^3 + \frac{2}{15}\hat{K}_2 v^5} \equiv v\, G(\varepsilon) , \tag{19}$$

$$C(v) \simeq \frac{2}{15} k_\perp^2 \rho_i^2 v^2 , \tag{20}$$

where $\varepsilon = v^2/2$ is the normalized energy, and a function, $G(\varepsilon)$, is introduced for simplicity. The critical energy of an ion, $E_c = m_i v_c^2/2 = v_c^2 T_i/2$, below

which the rate of slowing down by ions exceeds that by electrons, is represented as

$$E_c = 14.8\ T_e \times A_i^{1/3}\Big(\sum_j \frac{n_j Z_j^2}{n_e}\frac{A_i}{A_j}\Big)^{2/3}\ , \tag{21}$$

where the summation is made over all ion species in a plasma. The argument of exp in Eq.(18) is expressed by the Taylor expansion at the normalized injection energy, $\varepsilon_0 = v_0^2/2$;

$$\int_{v_0}^{v} dv'\ A(v') = \int_{\varepsilon_0}^{\varepsilon} d\varepsilon'\ G(\varepsilon')$$
$$= (\varepsilon-\varepsilon_0)G(\varepsilon_0) + \frac{1}{2}(\varepsilon-\varepsilon_0)^2\frac{dG(\varepsilon_0)}{d\varepsilon} + \cdots . \tag{22}$$

If we consider the case of $\hat{T}_{1/e}/\varepsilon_0 \ll 1$, we can easily evaluate the "extended-tail temperature" from Eqs.(16), (18), and (22) as

$$\hat{T}_{1/e}\ G(\varepsilon_0) = 1\ , \tag{23}$$

which gives a linear relation between $\hat{K}_2$ and $\Delta\hat{T}_{1/e}$;

$$\hat{K}_2 = \frac{15}{2}\ \frac{v_0^3 + v_c^3}{v_0^5}\ \Delta\hat{T}_{1/e}\ . \tag{24}$$

Next we seek the approximated expression for $\hat{P}_{RF}$ given by Eq.(15). As is shown in Fig.1, the high energy tail above $v_0^2/2$ is appreciably modified by RF-induced diffusion, while the distribution function below $v_0^2/2$ is almost unchanged by the ICRF wave. Therefore, the distribution function is approximated as

$$F_0(v) = \frac{1-\sigma_{tail}}{(2\pi)^{3/2}}\exp\Big(-\frac{v^2}{2}\Big) + \frac{\hat{P}_{NBI}}{4\pi\varepsilon_0}\ \frac{1}{v^3+v_c^3}\ U(v_0-v)$$
$$+ \frac{\hat{P}_{NBI}}{4\pi\varepsilon_0}\ \frac{1}{v_0^3+v_c^3}\exp\Big(-\frac{v^2-v_0^2}{2\hat{T}_{1/e}}\Big)\ U(v-v_0)\ , \tag{25}$$

where σ_{tail} is the density fraction of the tail component,

$$\sigma_{tail} = \frac{\hat{P}_{NBI}}{\varepsilon_0}\left[\frac{1}{3}\ln\frac{v_0^3+v_c^3}{v_c^3} + \hat{T}_{1/e}\frac{v_0}{v_0^3+v_c^3} + \sqrt{\frac{\pi}{2}}\frac{(\hat{T}_{1/e})^{3/2}}{v_0^3+v_c^3}\exp\left(\frac{v_0^2}{2\hat{T}_{1/e}}\right)\left\{1-\Phi\left(\frac{v_0}{\sqrt{2\hat{T}_{1/e}}}\right)\right\}\right],$$

$$\simeq \frac{\hat{P}_{NBI}}{\varepsilon_0}\left[\frac{1}{3}\ln\frac{v_0^3+v_c^3}{v_c^3} + \hat{T}_{1/e}\frac{v_0}{v_0^3+v_c^3} + \frac{(\hat{T}_{1/e})^2}{v_0(v_0^3+v_c^3)}\right], \qquad (26)$$

which is subject to particle conservation. Here, $\Phi(x)$ is the error function.

By inserting Eqs.(20), (24), (25), and (26) into Eq.(15), we obtain the deposited RF power density as a function of $\Delta\hat{T}_{1/e}$ through tedious but straightforward calculation;

$$\hat{P}_{RF} = \frac{15}{2}\frac{\Delta\hat{T}_{1/e}}{\varepsilon_0}(1+\lambda^3)\left[\left(1-\frac{1}{3}\frac{\hat{P}_{NBI}}{\varepsilon_0}\ln\frac{1+\lambda^3}{\lambda^3}\right) + \frac{1}{3}\hat{P}_{NBI}\left\{1+\frac{\lambda^2}{3}\ln\frac{(1+\lambda)^3}{1+\lambda^3} - \frac{2\lambda^2}{\sqrt{3}}\left(\tan^{-1}\frac{2-\lambda}{\sqrt{3}\lambda}+\frac{\pi}{6}\right)\right\}\right]$$

$$+ \frac{15}{2}\frac{\Delta T_{1/e}}{\varepsilon_0}\hat{P}_{NBI}\left[\left(\frac{2}{3}-\frac{1}{\varepsilon_0}\right)\frac{\hat{T}_{1/e}^{beam}+\Delta\hat{T}_{1/e}}{2\varepsilon_0} + \left(2-\frac{1}{\varepsilon_0}\right)\frac{(\hat{T}_{1/e}^{beam}+\Delta\hat{T}_{1/e})^2}{4\varepsilon_0^2} + \frac{(\hat{T}_{1/e}^{beam}+\Delta\hat{T}_{1/e})^3}{4\varepsilon_0^3}\right], \qquad (27)$$

where $\lambda = v_c / v_0$. It must be noted that this equation is applicable for $T_{1/e} \ll E_0$. When $\hat{P}_{NBI} \ll 3$, Eq.(27) is simplified as

$$\Delta T_{1/e} \simeq \frac{2E_0}{15(1+\lambda^3)}\hat{P}_{RF}\left(1-\frac{1}{3}\frac{\hat{P}_{NBI}}{\varepsilon_0}\ln\frac{1+\lambda^3}{\lambda^3}\right)^{-1}, \qquad (28)$$

which shows the n_e^{-2} dependence of $\Delta T_{1/e}$ (see Eq.(14) for $\hat{P}$). On the other hand, $\Delta T_{1/e}$ becomes independent of n_e for $\hat{P}_{NBI} \gg 3$;

$$\Delta T_{1/e} \simeq \frac{2E_0}{5(1+\lambda^3)}\frac{\hat{P}_{RF}}{\hat{P}_{NBI}}\left\{1+\frac{\lambda^2}{3}\ln\frac{(1+\lambda)^3}{1+\lambda^3} - \frac{2\lambda^2}{\sqrt{3}}\left(\tan^{-1}\frac{2-\lambda}{\sqrt{3}\lambda}+\frac{\pi}{6}\right)\right\}^{-1}, \qquad (29)$$

where $T_{1/e}/E_0 \ll 1$ is assumed.

Figure 3 shows $\Delta\hat{T}_{1/e}$ versus $\hat{P}_{RF}$. Parameters are the same as those for Figs.1 and 2; $T_e/T_i = 1.1$, $E_0/T_i = 20$, and $\hat{P}_{NBI} = 4$. The results by the exact solution (Eq.(13)) in Section 2 and approximated ones (Eq.(27)) are plotted by the dashed line and the solid line, respectively. An excellent agreement is seen between them except in the higher $\hat{P}_{RF}$ region

or the larger $T_{1/e}/E_0$ region. Deviation of the approximated results from the exact ones mainly comes from lower estimation of the deposited RF power density, which is attributed to the insufficient expression of $F_0(v)$ for $v \geqq v_0$ in Eq.(25).

4. NUMERICAL ANALYSIS

We study the ion tail formation by using a two-dimensional linearized Fokker-Planck code. Stationary results are found from the time dependent calculation. We investigate the "extended-tail temperature" for the angle-averaged distribution, $F_0(v)$, and that for the distribution, $f(v,\theta_{obs})$, at an azimuthal angle, $\theta = \theta_{obs}$. The plasma parameter and the NBI parameters are the same as those for Figs.1 and 2; $T_e/T_i = 1.1$, $E_0/T_i = 20$, and $\hat{P}_{NBI} = 4$.

In Fig.3 the increment of the "extended-tail temperature", $\Delta\hat{T}_{1/e}$, for the angle-averaged distribution is plotted as a function of the deposited RF power density, $\hat{P}_{RF}$. The injection angle, θ_0, is varied as $\theta_0 = \pm 50^\circ$ (square), $\theta_0 = \pm 70^\circ$ (cross), and $\theta_0 = 90^\circ$ (triangle). The result for the nearly-perpendicular injection ($\theta_0 = \pm 70^\circ$) is in good agreement with the analytical results (solid and dashed lines). For the case of $\theta_0 = 90^\circ$, $\Delta\hat{T}_{1/e}$ becomes larger than the analytical ones, and that for $\theta_0 = \pm 50^\circ$ becomes smaller. The relative difference is about 30%.

Next, we study the dependence of $\Delta\hat{T}_{1/e}$ on the observation angle, θ_{obs}. Figure 4(a) shows contour lines of the distribution function in ($v_\parallel$, $v_\perp$) space. The injection angle is chosen as $\theta_0 = \pm 70^\circ$, and $\hat{P}_{RF} = 3$. The observation lines, $\theta_{obs} = 60^\circ$, 70°, and 80°, are given by dashed lines. The distribution has the local maxima at the injection points, $v = 6.32$ and $\theta = \pm 70^\circ$. A large amount of anisotropy due to RF-induced diffusion is seen from the figure. The distribution functions, $f(v^2/2,\theta_{obs})$, for three θ_{obs} values are also demonstrated in Fig.4(b), where $F_0(v^2/2)$ is shown for comparison. The "extended-tail temperature" at $\theta_{obs} = 80^\circ$ is significantly enhanced by RF-induced diffusion, while $\Delta\hat{T}_{1/e}$ at $\theta_{obs} = 60^\circ$ is lower than that for the angle-averaged distribution. At the injection angle, $\theta_{obs} = \theta_0 = 70^\circ$, $\Delta\hat{T}_{1/e}$ becomes especially low, though the higher energy tail for $\theta_{obs} = 70^\circ$ is enhanced more significantly than that for $\theta_{obs} = 60^\circ$. This is interpreted as follows: Since the direction of RF-induced diffusion is perpendicular to the magnetic field, the RF effects on the high energy tail become much appreciable as θ_{obs} approaches $\pi/2$. For $\theta_{obs} = \theta_0 = 70^\circ$, however, the height of the distribution function at the injection speed,

or the larger $T_{1/e}/E_0$ region. Deviation of the approximated results from the exact ones mainly comes from lower estimation of the deposited RF power density, which is attributed to the insufficient expression of $F_0(v)$ for $v \geqq v_0$ in Eq.(25).

4. NUMERICAL ANALYSIS

We study the ion tail formation by using a two-dimensional linearized Fokker-Planck code. Stationary results are found from the time dependent calculation. We investigate the "extended-tail temperature" for the angle-averaged distribution, $F_0(v)$, and that for the distribution, $f(v,\theta_{obs})$, at an azimuthal angle, $\theta = \theta_{obs}$. The plasma parameter and the NBI parameters are the same as those for Figs.1 and 2; $T_e/T_i = 1.1$, $E_0/T_i = 20$, and $\hat{P}_{NBI} = 4$.

In Fig.3 the increment of the "extended-tail temperature", $\Delta\hat{T}_{1/e}$, for the angle-averaged distribution is plotted as a function of the deposited RF power density, $\hat{P}_{RF}$. The injection angle, θ_0, is varied as $\theta_0 = \pm 50^\circ$ (square), $\theta_0 = \pm 70^\circ$ (cross), and $\theta_0 = 90^\circ$ (triangle). The result for the nearly-perpendicular injection ($\theta_0 = \pm 70^\circ$) is in good agreement with the analytical results (solid and dashed lines). For the case of $\theta_0 = 90^\circ$, $\Delta\hat{T}_{1/e}$ becomes larger than the analytical ones, and that for $\theta_0 = \pm 50^\circ$ becomes smaller. The relative difference is about 30%.

Next, we study the dependence of $\Delta\hat{T}_{1/e}$ on the observation angle, θ_{obs}. Figure 4(a) shows contour lines of the distribution function in ($v_\parallel$, $v_\perp$) space. The injection angle is chosen as $\theta_0 = \pm 70^\circ$, and $\hat{P}_{RF} = 3$. The observation lines, $\theta_{obs} = 60^\circ$, 70°, and 80°, are given by dashed lines. The distribution has the local maxima at the injection points, $v = 6.32$ and $\theta = \pm 70^\circ$. A large amount of anisotropy due to RF-induced diffusion is seen from the figure. The distribution functions, $f(v^2/2,\theta_{obs})$, for three θ_{obs} values are also demonstrated in Fig.4(b), where $F_0(v^2/2)$ is shown for comparison. The "extended-tail temperature" at $\theta_{obs} = 80^\circ$ is significantly enhanced by RF-induced diffusion, while $\Delta\hat{T}_{1/e}$ at $\theta_{obs} = 60^\circ$ is lower than that for the angle-averaged distribution. At the injection angle, $\theta_{obs} = \theta_0 = 70^\circ$, $\Delta\hat{T}_{1/e}$ becomes especially low, though the higher energy tail for $\theta_{obs} = 70^\circ$ is enhanced more significantly than that for $\theta_{obs} = 60^\circ$. This is interpreted as follows: Since the direction of RF-induced diffusion is perpendicular to the magnetic field, the RF effects on the high energy tail become much appreciable as θ_{obs} approaches $\pi/2$. For $\theta_{obs} = \theta_0 = 70^\circ$, however, the height of the distribution function at the injection speed,

v_0, tends to be raised by the point source of NBI. This leads to the sharp slope of the distribution at v_0, and hence to the smaller "extended-tail temperature". Relations between $\hat{P}_{RF}$ and $\Delta\hat{T}_{1/e}$ for the distributions, $f(v,\theta_{obs})$, at θ_{obs} = 60° (circle), 70° (triangle), and 80° (square) are shown in Fig.5. The temperature increment, $\Delta\hat{T}_{1/e}$, as a function of $\hat{P}_{RF}$ for $f(v,\theta_{obs})$ strongly depends upon θ_{obs}. The scaling of the "extended-tail temperature" for each $f(v,\theta_{obs})$ should contain the effect of anisotropy of the distribution. The temperature increment, $\Delta\hat{T}_{1/e}$, for $F_0(v)$ and $\overline{F}(v)$ averaged over θ = 60° - 90° are also plotted by crosses and by asterisks, respectively. Although $\Delta\hat{T}_{1/e}$ for $f(v,\theta_{obs})$ is much different from that for $F_0(v)$, $\Delta\hat{T}_{1/e}$ for $\overline{F}(v)$ agrees fairly well with that for $F_0(v)$. These numerical results indicate that a averaging disposition of experimental data over θ_{obs} is necessary for the data analysis by using the scaling, Eq.(27). The deposition of NBI and ICRF heating power is spatially spread in a tokamak plasma. A charge-exchange neutral particle pointing to the direction of a diagnostic port corresponds to an ion with a pitch angle, θ_{obs}, which is determined by a radial position of the charge-exchange reaction. Therefore, the averaging disposition is automatically brought about by this spatial effect in usual experiments.

5. DISCUSSION

Recently, combined NBI and ICRF heating experiments were performed in JT-60. The significant increase of the "extended-tail temperature" was observed, and a linear relation of $\Delta T_{1/e} \propto \tau_s$ was found [8]. It was further confirmed that the beam acceleration by ICRF occurs in the plasma core. The radial spread of the power deposition region leads to spread in θ_{obs} of the measured spectrum. Then, the angle-averaged distribution may be useful to estimate the "extended-tail temperature". Now, we compare these experimental results with the present scaling, Eq.(27). We consider the following situation: The hydrogen beam with E_0 = 60 keV is injected into a hydrogen plasma with low impurity concentration (A_i = 1, Z_i = 1, and $n_i = n_e$). The power densities deposited near the plasma center are P_{NBI} = 0.2 W/cm^3 and P_{RF} = 0.3 W/cm^3. Since we take notice of the relation between τ_s and $\Delta T_{1/e}$, we change values of n_e and T_e with fixed T_i of 3 keV.

Figure 6 shows (a) $\Delta T_{1/e}$ versus n_e and (b) $\Delta T_{1/e}$ versus τ_s, which are obtained from Eq.(27). Although $\Delta T_{1/e}$ decreases with n_e and increases with T_e, the dependence of $\Delta T_{1/e}$ on τ_s is not unique. The result in Ref.[8] of $\Delta T_{1/e} \propto \tau_s$ may come from special experimental conditions. In JT-60

v_0, tends to be raised by the point source of NBI. This leads to the sharp slope of the distribution at v_0, and hence to the smaller "extended-tail temperature". Relations between $\hat{P}_{RF}$ and $\Delta\hat{T}_{1/e}$ for the distributions, $f(v,\theta_{obs})$, at θ_{obs} = 60° (circle), 70° (triangle), and 80° (square) are shown in Fig.5. The temperature increment, $\Delta\hat{T}_{1/e}$, as a function of $\hat{P}_{RF}$ for $f(v,\theta_{obs})$ strongly depends upon θ_{obs}. The scaling of the "extended-tail temperature" for each $f(v,\theta_{obs})$ should contain the effect of anisotropy of the distribution. The temperature increment, $\Delta\hat{T}_{1/e}$, for $F_0(v)$ and $\overline{F}(v)$ averaged over θ = 60° - 90° are also plotted by crosses and by asterisks, respectively. Although $\Delta\hat{T}_{1/e}$ for $f(v,\theta_{obs})$ is much different from that for $F_0(v)$, $\Delta\hat{T}_{1/e}$ for $\overline{F}(v)$ agrees fairly well with that for $F_0(v)$. These numerical results indicate that a averaging disposition of experimental data over θ_{obs} is necessary for the data analysis by using the scaling, Eq.(27). The deposition of NBI and ICRF heating power is spatially spread in a tokamak plasma. A charge-exchange neutral particle pointing to the direction of a diagnostic port corresponds to an ion with a pitch angle, θ_{obs}, which is determined by a radial position of the charge-exchange reaction. Therefore, the averaging disposition is automatically brought about by this spatial effect in usual experiments.

5. DISCUSSION

Recently, combined NBI and ICRF heating experiments were performed in JT-60. The significant increase of the "extended-tail temperature" was observed, and a linear relation of $\Delta T_{1/e} \propto \tau_s$ was found [8]. It was further confirmed that the beam acceleration by ICRF occurs in the plasma core. The radial spread of the power deposition region leads to spread in θ_{obs} of the measured spectrum. Then, the angle-averaged distribution may be useful to estimate the "extended-tail temperature". Now, we compare these experimental results with the present scaling, Eq.(27). We consider the following situation: The hydrogen beam with E_0 = 60 keV is injected into a hydrogen plasma with low impurity concentration (A_i = 1, Z_i = 1, and $n_i = n_e$). The power densities deposited near the plasma center are P_{NBI} = 0.2 W/cm^3 and P_{RF} = 0.3 W/cm^3. Since we take notice of the relation between τ_s and $\Delta T_{1/e}$, we change values of n_e and T_e with fixed T_i of 3 keV.

Figure 6 shows (a) $\Delta T_{1/e}$ versus n_e and (b) $\Delta T_{1/e}$ versus τ_s, which are obtained from Eq.(27). Although $\Delta T_{1/e}$ decreases with n_e and increases with T_e, the dependence of $\Delta T_{1/e}$ on τ_s is not unique. The result in Ref.[8] of $\Delta T_{1/e} \propto \tau_s$ may come from special experimental conditions. In JT-60

heating experiments, the relation of $T_e \propto n_e^{-1/3}$ has been obtained empirically, and the experimental results, $\Delta T_{1/e} \propto \tau_s$, reduces to $\Delta T_{1/e} \propto n_e^{-3/2}$. Therefore we adjust the analytical results by using this relation. The n_e-dependence and the τ_s-dependence of $\Delta T_{1/e}$ given by Eq.(27) under the relation, $T_e \propto n_e^{-1/3}$, are shown by asterisks in the figures. The reference point is chosen at $n_e = 2.7\times10^{12}$ cm^{-3} and $T_e = 3.4$ keV, and Eq.(27) gives $\Delta T_{1/e} = 15.9$ keV at this point (the parameters used in the former sections, $T_e/T_i = 1.1$, $E_0/T_i = 20$, and $\hat{P}_{NBI} = 4$, correspond to this reference point). A thick curve, $\Delta T_{1/e} \propto n_e^{-3/2}$, in Fig.6(a) and a thick straight line, $\Delta T_{1/e} \propto \tau_s$, in Fig.6(b) are drawn from each reference point, which well fit the analytical results indicated by asterisks except in the low density region. This fact is explained as follows: If T_e is proportional to $n_e^{-\alpha}$ ($\alpha > 0$) for fixed values of P_{NBI}, P_{RF}, and T_i, Eqs.(29) and (28) show that the n_e-dependence of $\Delta T_{1/e}/\tau_s$ varies from $n_e^{3\alpha/2+1}$ to n_e^{-1} around $\hat{P}_{NBI} = 3$, and the linear relation, $\Delta T_{1/e} \propto \tau_s$, can be seen in the transient region. Thus, $\Delta T_{1/e}$ is approximately proportional to τ_s as was found in Ref.[8], for the case of fixed P_{NBI}, P_{RF}, and T_i, and of $T_e \propto n_e^{-1/3}$ in the density range, 2.5×10^{13} cm^{-3} $< n_e <$ 6.5×10^{13} cm^{-3}.

Figure 7 shows the experimentally observed n_e-dependence of $\Delta T_{1/e}$ with the NBI power of $\mathcal{P}_{NBI} = 4.9 - 6$ MW and the ICRF power of $\mathcal{P}_{RF} = 1.2 - 1.3$ MW. The results for $(\Delta\varphi=\pi, \Delta\Theta=0)$ phasing are plotted by open circles, where $(\Delta\varphi, \Delta\Theta)$ indicates the toroidal and poloidal phase differences of the 2×2 loop antenna array. The black circle is for (0,0) phasing. These experimental data were rearranged as the τ_s-dependence of ΔT_i^{tail} ($\equiv \Delta T_{1/e}$) in Fig.3(a) of Ref.[8]. The crosses are based on the scaling, Eq.(27), where values of n_e and T_e are chosen as the same as the experimental ones while T_i is fixed 3 keV. The NBI power of $\mathcal{P}_{NBI} = 5$ MW and the ICRF power of $\mathcal{P}_{RF} = 1.2$ MW are converted into the beam power density of $P_{NBI} = 0.2$ W/cm^3 and the RF power density of $P_{RF} = 0.25$ W/cm^3, respectively. The values based on the scaling are consistent with the experimental ones for $(\pi,0)$ phasing. From the difference between the experimental result for (0,0) phasing and the corresponding theoretical one, the conversion rate of the ICRF power into the power density will be of the order of one third of that for $(\pi,0)$ phasing. This comes from the fact that the power deposition profile becomes more centrally-peaked for $(\pi,0)$ phasing than that for (0,0) phasing [8].

The dependence of $\Delta T_{1/e}$ on $\mathcal{P}_{NBI}$ was also studied experimentally for (0,0) phasing with $\mathcal{P}_{RF} = 1.7$ MW, and the result was shown in Fig.20 of Ref.[9]. In Fig.8, we plot the $\mathcal{P}_{NBI}$-dependence of $\Delta T_{1/e}$ based on the scaling, Eq.(27), by crosses with these experimental data (circles). The values

of n_e and T_e are chosen as the same as the experimental ones while T_i is fixed 3 keV. The RF power density, P_{RF}, is 0.12 W/cm^3. The conversion rate of $\mathcal{P}_{NBI}$ into P_{NBI} is the same as in Fig.7. The conversion rate of $\mathcal{P}_{RF}$ into P_{RF} is one third of that for $(\pi,0)$ phasing. The theoretical values based on the scaling agree fairly well with the experimental ones. It is confirmed that $\Delta T_{1/e}$ is almost independent of $\mathcal{P}_{NBI}$.

In this way, the present scaling of the "extended-tail temperature" given by Eq.(27) is consistent with the data of the combined heating experiments in JT-60, although the scaling is derived on the basis of the fairly rough model.

6. CONCLUSION

The enhancement of the beam-induced tail temperature by the second harmonic ICRF waves has been investigated. A simple scaling of the "extended-tail temperature" for an angle-averaged distribution with respect to the deposited RF power density is presented. Numerical results for nearly-perpendicular beam injection are in good agreement with 1D analysis. The simple scaling is also consistent with the data of combined heating experiments in JT-60. The present analysis is useful to estimate the coupled RF power density from the charge-exchange spectra. In the present calculation the angle-averaged distribution is assumed to correspond to the charge-exchange spectra. The exact bounce-average aspect including the trapped particle effect on the "extended-tail temperature" is left for future study.

ACKNOWLEDGEMENT

We wish to thank Drs. M. Nagami, K. Hamamatsu, R. Yoshino, K. Tani, and Y. Shimomura for valuable discussions. We are grateful to Drs. K. Tobita, Y. Kusama, and M. Nemoto for helpful discussion of charge-exchange neutral measurements. The continuous encouragement by Drs. T. Takeda, M. Tanaka, and M. Yoshikawa is also appreciated.

of n_e and T_e are chosen as the same as the experimental ones while T_i is fixed 3 keV. The RF power density, P_{RF}, is 0.12 W/cm^3. The conversion rate of $\mathcal{P}_{NBI}$ into P_{NBI} is the same as in Fig.7. The conversion rate of $\mathcal{P}_{RF}$ into P_{RF} is one third of that for $(\pi,0)$ phasing. The theoretical values based on the scaling agree fairly well with the experimental ones. It is confirmed that $\Delta T_{1/e}$ is almost independent of $\mathcal{P}_{NBI}$.

In this way, the present scaling of the "extended-tail temperature" given by Eq.(27) is consistent with the data of the combined heating experiments in JT-60, although the scaling is derived on the basis of the fairly rough model.

6. CONCLUSION

The enhancement of the beam-induced tail temperature by the second harmonic ICRF waves has been investigated. A simple scaling of the "extended-tail temperature" for an angle-averaged distribution with respect to the deposited RF power density is presented. Numerical results for nearly-perpendicular beam injection are in good agreement with 1D analysis. The simple scaling is also consistent with the data of combined heating experiments in JT-60. The present analysis is useful to estimate the coupled RF power density from the charge-exchange spectra. In the present calculation the angle-averaged distribution is assumed to correspond to the charge-exchange spectra. The exact bounce-average aspect including the trapped particle effect on the "extended-tail temperature" is left for future study.

ACKNOWLEDGEMENT

We wish to thank Drs. M. Nagami, K. Hamamatsu, R. Yoshino, K. Tani, and Y. Shimomura for valuable discussions. We are grateful to Drs. K. Tobita, Y. Kusama, and M. Nemoto for helpful discussion of charge-exchange neutral measurements. The continuous encouragement by Drs. T. Takeda, M. Tanaka, and M. Yoshikawa is also appreciated.

of n_e and T_e are chosen as the same as the experimental ones while T_i is fixed 3 keV. The RF power density, P_{RF}, is 0.12 W/cm^3. The conversion rate of $\mathcal{P}_{NBI}$ into P_{NBI} is the same as in Fig.7. The conversion rate of $\mathcal{P}_{RF}$ into P_{RF} is one third of that for $(\pi,0)$ phasing. The theoretical values based on the scaling agree fairly well with the experimental ones. It is confirmed that $\Delta T_{1/e}$ is almost independent of $\mathcal{P}_{NBI}$.

In this way, the present scaling of the "extended-tail temperature" given by Eq.(27) is consistent with the data of the combined heating experiments in JT-60, although the scaling is derived on the basis of the fairly rough model.

6. CONCLUSION

The enhancement of the beam-induced tail temperature by the second harmonic ICRF waves has been investigated. A simple scaling of the "extended-tail temperature" for an angle-averaged distribution with respect to the deposited RF power density is presented. Numerical results for nearly-perpendicular beam injection are in good agreement with 1D analysis. The simple scaling is also consistent with the data of combined heating experiments in JT-60. The present analysis is useful to estimate the coupled RF power density from the charge-exchange spectra. In the present calculation the angle-averaged distribution is assumed to correspond to the charge-exchange spectra. The exact bounce-average aspect including the trapped particle effect on the "extended-tail temperature" is left for future study.

ACKNOWLEDGEMENT

We wish to thank Drs. M. Nagami, K. Hamamatsu, R. Yoshino, K. Tani, and Y. Shimomura for valuable discussions. We are grateful to Drs. K. Tobita, Y. Kusama, and M. Nemoto for helpful discussion of charge-exchange neutral measurements. The continuous encouragement by Drs. T. Takeda, M. Tanaka, and M. Yoshikawa is also appreciated.

REFERENCES

[1] OKANO, K., INOUE, N., UCHIDA, T., Nucl. Fusion 23 (1983) 235.

[2] COX, M., START, D.F.H., Nucl. Fusion 24 (1984) 399.

[3] KESNER, J., Nucl. Fusion 18 (1978) 781.

[4] PEKKARI, L.O., ANDERSON, D., HAMNEN, H., LISAK, M., Nucl. Fusion 23 (1983) 781.

[5] YAMAGIWA, M., TAKIZUKA, T., KISHIMOTO, Y., Fusion Reactivity Enhancement due to Ion Tail Formation by Beam and Ion Cyclotron Heating, Japan Atomic Energy Research Institute, Rep. JAERI-M 87-065.

[6] HWANG, D., BITTER, M., BUDNY, R., CAVALLO, A., et al., in Plasma Physics and Controlled Nuclear Fusion Research (Proc. 9th Int. Conf. Baltimore, 1982) Vol.2, IAEA, Vienna (1983) 3.

[7] JACQUINOT, J., JET Team, 11th Conf. on Plasma Physics and Controlled Nuclear Fusion Research, Kyoto, 1986, paper IAEA-CN-47/F-I-1.

[8] KIMURA, H., JT-60 Team, Proc. 14th Europ. Conf. on Controlled Fusion and Plasma Physics, Madrid, 1987, 11D, Part III (1987) 857.

[9] YOSHINO, R., JT-60 Team, invited paper, 14th Europ. Conf. on Controlled Fusion and Plasma Physics, Madrid, 1987.

[10] HINTON, F.L., 'Collisional Transport in Plasma' in Handbook of Plasma Physics, ed. M.N. Rosenbluth and R.Z. Sagdeev, North-Holland Publishing Company, Amsterdam, New York, Oxford (1983) Vol. 1, Chap. 1.5.

[11] RAM, A., BERS, A., Nucl. Fusion 24 (1984) 679.

[12] STIX, T.H., The Theory of Plasma Waves, McGraw-Hill, New York (1962).

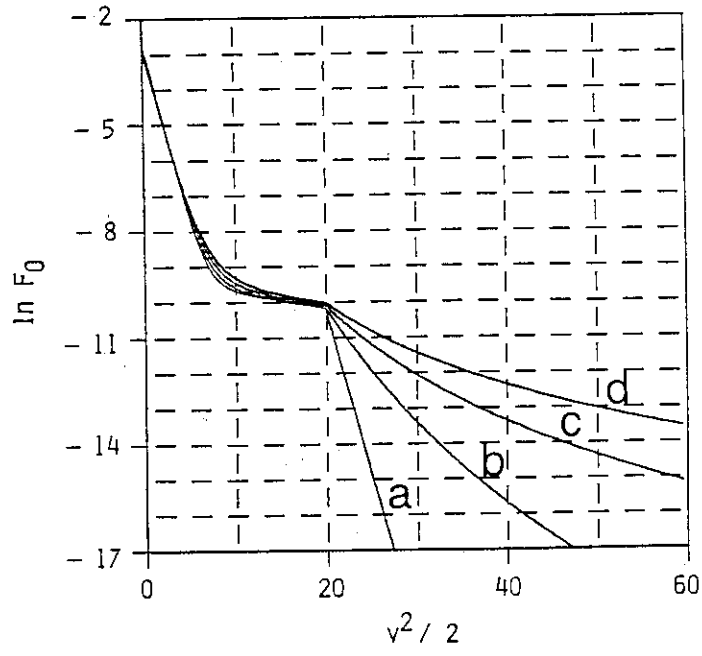

Fig. 1 Angle-averaged distribution function, $F_0(v^2/2)$, for combined NBI and ICRF heating. Energy is normalized by T_i. Parameters are T_e/T_i = 1.1, E_0/T_i = 20, $\hat{P}_{NBI}$ = 4, and $\hat{K}_2$ is varied as (a) 0, (b) 0.5, (c) 1.0, and (d) 1.5.

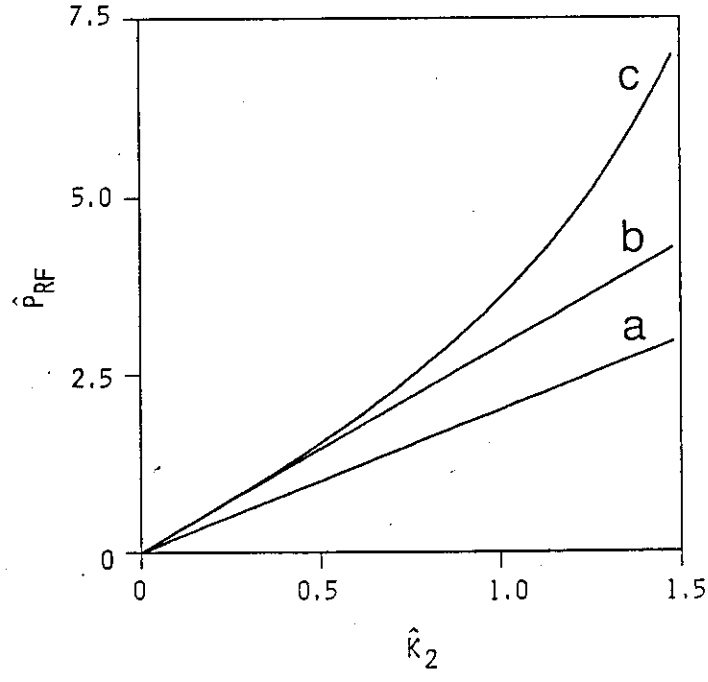

Fig. 2 Dependence of $\hat{P}_{RF}$ on $\hat{K}_2$. Parameters are the same as those for Fig. 1 except values of $\hat{K}_2$. (a) $\langle\hat{P}_{RF}\rangle_M$ (= 2 $\hat{K}_2$) is deposited RF power density for fixed Maxwellian distribution, (b) $\langle\hat{P}_{RF}\rangle_B$ for fixed distribution with only beam-induced tail, and (c) $\hat{P}_{RF}$ for exact distribution given by Eq.(13).

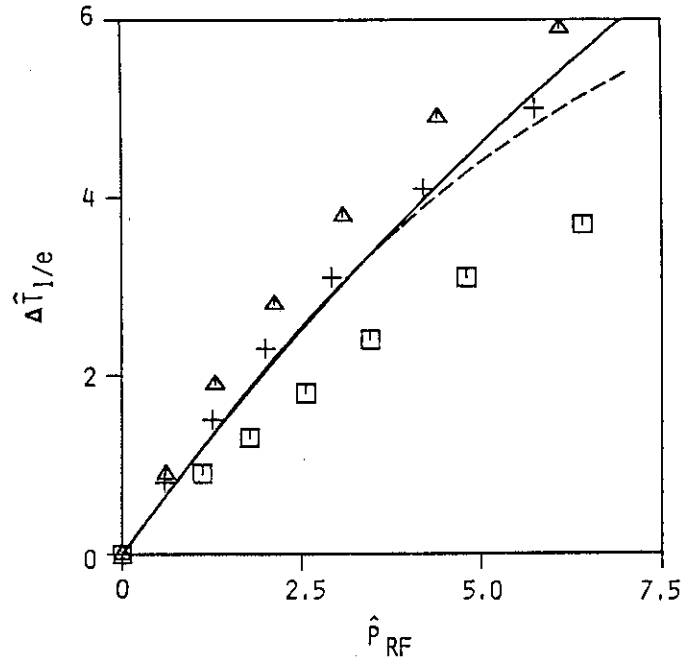

Fig. 3 Relation between $\hat{P}_{RF}$ and $\Delta\hat{T}_{1/e}$. Parameters are the same as those for Figs. 1 and 2. Analytical result by exact solution in Section 2 is shown by dashed line, and approximated relation of Eq.(27) is shown by solid line. Also shown are 2D numerical results of $\Delta\hat{T}_{1/e}$ for $F_0(v)$. Injection angles are $\theta_0 = \pm 50°$ (square), $\pm 70°$ (cross), and $90°$ (triangle).

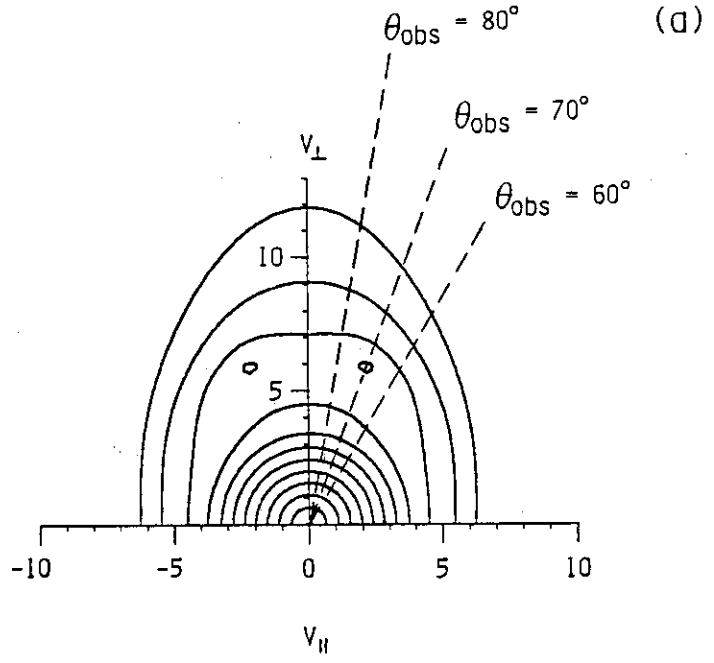

Fig. 4(a) Contour lines of distribution function in ($v_{//}$, $v_\perp$) space for combined NBI and ICRF heating. Parameters are $T_e/T_i = 1.1$, $E_0/T_i = 20$, $\hat{P}_{NBI} = 4$, $\theta_0 = \pm 70°$, and $\hat{P}_{RF} = 3$. Observation lines for $\theta_{obs} = 60°$, $70°$, and $80°$ are given by dashed lines.

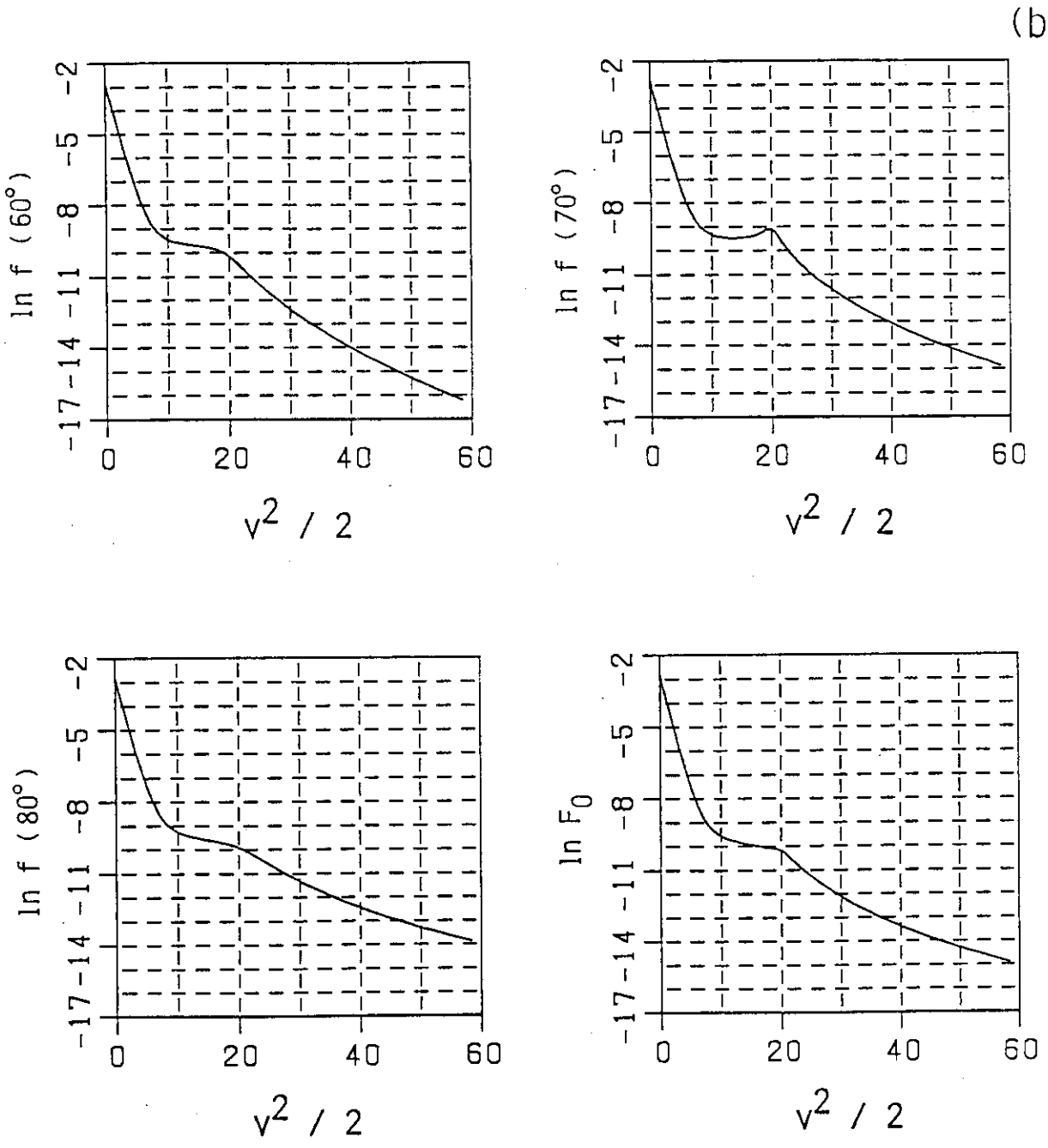

Fig. 4(b) Distribution functions, $f(v^2/2, \theta_{obs})$, at θ_{obs} = 60°, 70°, and 80°, and $F_0(v^2/2)$. Parameters are the same as those for Fig.4(a).

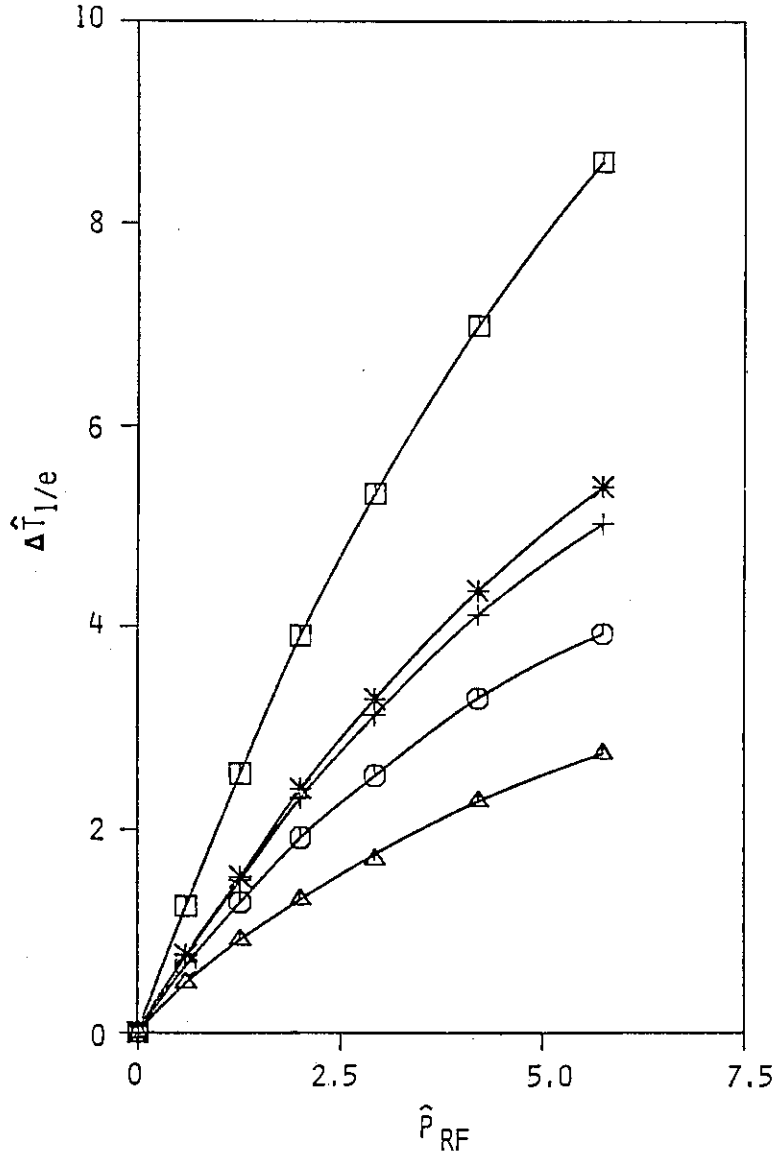

Fig. 5 Relation between $\hat{P}_{RF}$ and $\Delta\hat{T}_{1/e}$ for distributions, $f(v,\theta_{obs})$, at θ_{obs} = 60° (circle), 70° (triangle), 80° (square), and for $F_0(v)$ (cross) and $\overline{F}(v)$ (asterisk). Parameters are the same as those for Fig. 4 except value of $\hat{P}_{RF}$.

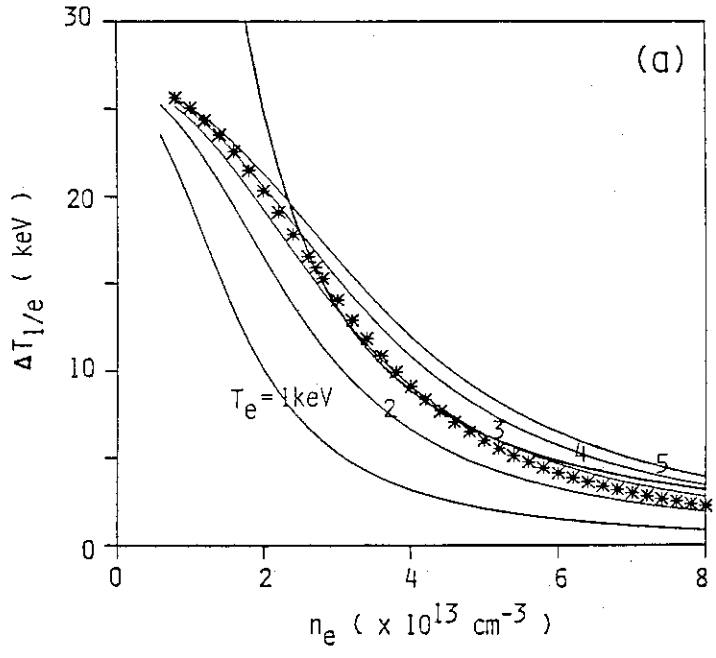

Fig. 6(a) Dependence of $\Delta T_{1/e}$ on n_e for various T_e values. Parameters are A_i = 1, Z_i = 1, $n_i = n_e$, T_i = 3 keV, E_0 = 60 keV, P_{NBI} = 0.2 W/cm^3, and P_{RF} = 0.3 W/cm^3. Asterisks show relations under constraint of $T_e \propto n_e^{-1/3}$. Thick line indicates $\Delta T_{1/e} \propto n_e^{-3/2}$.

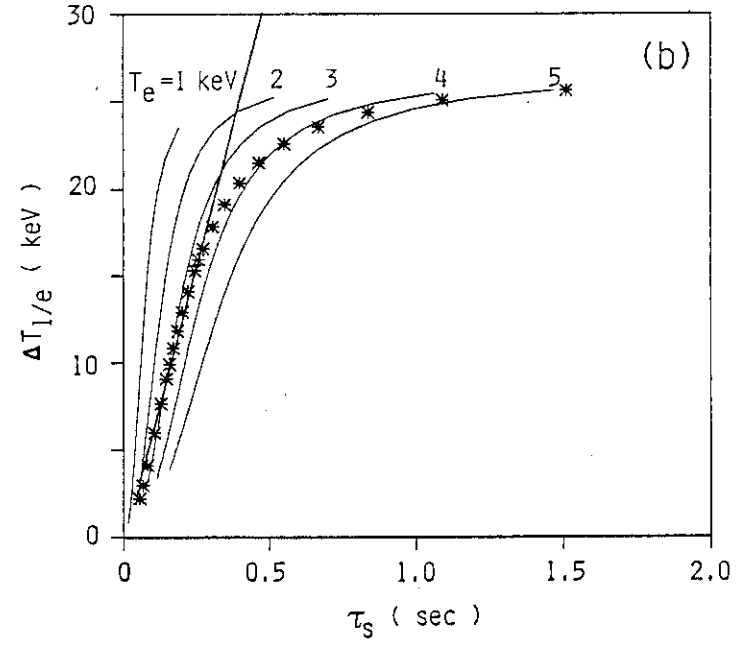

Fig. 6(b) Dependence of $\Delta T_{1/e}$ on τ_s for various T_e values. Parameters are the same as those for Fig.6(a). Asterisks show relations under constraint of $T_e \propto n_e^{-1/3}$. Thick line indicates $\Delta T_{1/e} \propto \tau_s$.

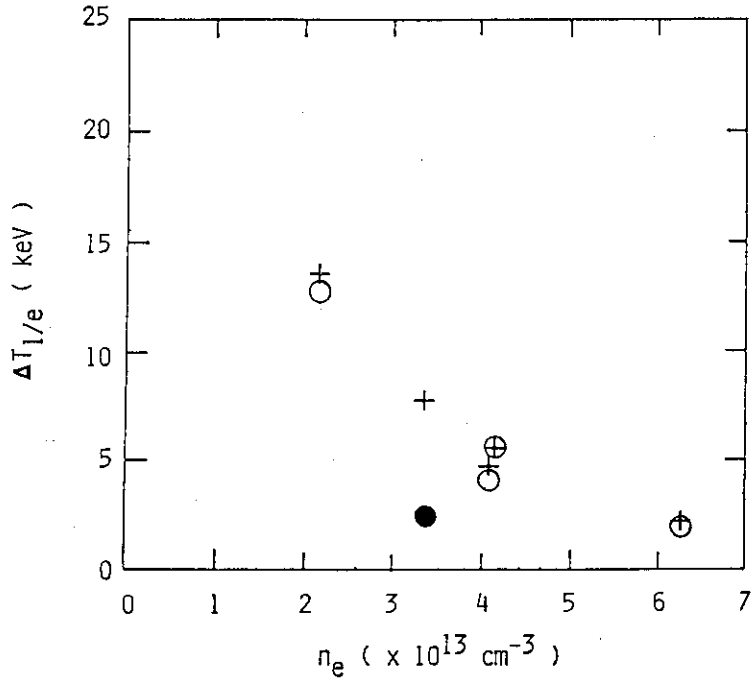

Fig. 7 Dependence of $\Delta T_{1/e}$ on n_e. Experimental values with $\mathcal{P}_{RF}$ = 1.2 - 1.3 MW and $\mathcal{P}_{NBI}$ = 4.9 - 6 MW are plotted by open circles for $(\pi,0)$ phasing and by black circle for (0,0) phasing. Crosses are based on the scaling, Eq.(27), with T_i of 3 keV. It is assumed that $\mathcal{P}_{NBI}$ = 5 MW and $\mathcal{P}_{RF}$ = 1.2 MW correspond to P_{NBI} = 0.2 W/cm^3 and P_{RF} = 0.25 W/cm^3, respectively.

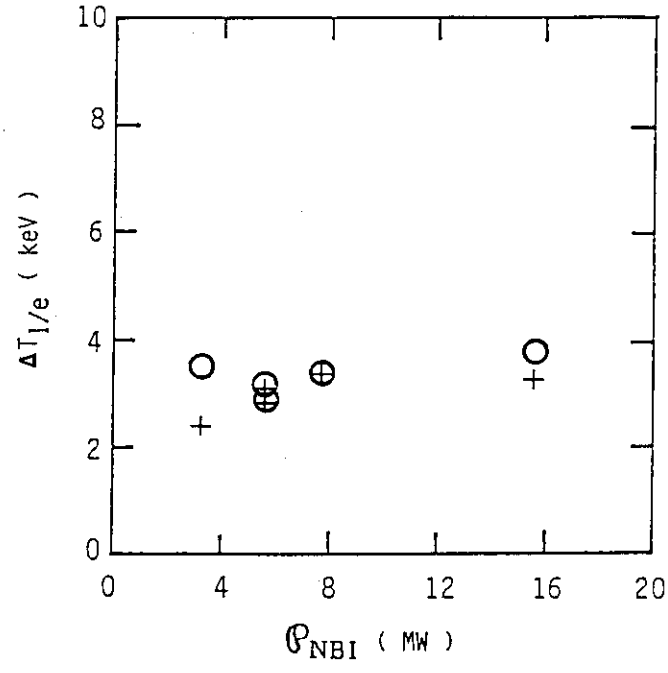

Fig. 8 Dependence of $\Delta T_{1/e}$ on $\mathcal{P}_{NBI}$. Experimental values for (0,0) phasing with $\mathcal{P}_{RF}$ = 1.7 MW are plotted by circles. Crosses are based on the scaling, Eq.(27), with T_i of 3 keV and P_{RF} of 0.12 W/cm^3. Conversion rate of $\mathcal{P}_{RF}$ into P_{RF} for (0,0) phasing is assumed to be one third of that for $(\pi,0)$ phasing in Fig.7, while the conversion rate of $\mathcal{P}_{NBI}$ into P_{NBI} is the same as in Fig.7.